ACS NANO

www.acsnano.org

ARTICLE

Criteria for Assessing the Interlayer Coupling of van der Waals Heterostructures Using Ultrafast Pump–Probe Photoluminescence Spectroscopy

Shuangping Han, Xilong Liang, Chengbing Qin,* Yan Gao, Yunrui Song, Shen Wang, Xingliang Su, Guofeng Zhang, Ruiyun Chen, Jianyong Hu, Mingyong Jing, Liantuan Xiao,* and Suotang Jia

Cite This: *ACS Nano* 2021, 15, 12966–12974

Read Online

ACCESS | Metrics & More | Article Recommendations | Supporting Information

ABSTRACT: van der Waals (vdW) heterostructures of transition metal dichalcogenides (TMDCs) provide an excellent paradigm for next-generation electronic and optoelectronic applications. However, the reproducible fabrications of vdW heterostructure devices and the boosting of practical applications are severely hindered by their unstable performance, due to the lack of criteria to assess the interlayer coupling in heterostructures. Here we propose a physical model involving ultrafast electron transfer in the heterostructures and provide two criteria, η (the ratio of the transferred electrons to the total excited electrons) and ζ (the relative photoluminescence variation), to evaluate the interlayer coupling by considering the electron transfer in TMDC heterostructures and numerically simulating the corresponding rate equations. We have proved the effectiveness and robustness of two criteria by measuring the pump–probe photoluminescence intensity of monolayer WS_2 in the WS_2/WSe_2 heterostructures. During thermal annealing of WS_2/WSe_2, ζ varies from negative to positive values and η changes between 0 and 4.5×10^{-3} as the coupling strength enhanced; both of them can well characterize the tuning of interlayer coupling. We also design a scheme to image the interlayer coupling by performing PL imaging at two time delays. Our scheme offers powerful criteria to assess the interlayer coupling in TMDC heterostructures, offering opportunities for the implementation of vdW heterostructures for broadband and high-performance electronic and optoelectronic applications.

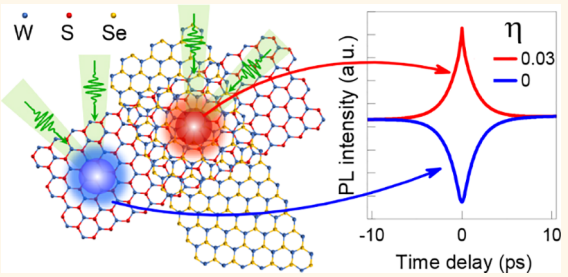

KEYWORDS: *vdW heterostructures, interlayer coupling strength, pump–probe, exciton relaxation time, criteria, PL intensity*

Two-dimensional (2D) transition metal dichalcogenide (TMDC) semiconductors have attracted significant research interest from the viewpoint of fundamental physics and for promising applications in various areas, resulting from their reduced dimensionality and crystal symmetry.[1−4] One of the most intriguing aspects of these 2D materials is that they provide an encouraging platform to fabricate multilayer structures by combining monolayers of different 2D materials via van der Waals (vdW) forces.[5−7] The so-called heterostructures constitute an excellent paradigm for promising electronic and optoelectronic applications, including superlattice Dirac points,[8] tunneling transistors,[9] light-emitting devices,[10] and ultrathin photodetectors.[11] Emergent properties of 2D heterostructures heavily rely on the interlayer electronic coupling, thus the ultrafast electron and energy transfer across the interface and interlayer coupling.[12] However, the presence of unwanted organic residues (such as poly(methyl methacrylate) (PMMA),[13] polypropylene carbonate (PPC),[14] and polydimethylsiloxane (PDMS)),[15] spatially inhomogeneous interfaces (such as blisters[16] or bubbles,[17] wrinkles,[18] and strain[19]), and crystal defects[20,21] is inevitable during the imperfect fabrications. The unpredictable interlayer coupling generally leads to unrepeatable or even incompatible experimental results.

To realize reproducible fabrications of vdW heterostructures and promote practical applications, two key elements should be explored. The first one is tuning the interlayer coupling as

Received: March 1, 2021
Accepted: July 23, 2021
Published: July 27, 2021

https://doi.org/10.1021/acsnano.1c01787
ACS Nano 2021, 15, 12966–12974

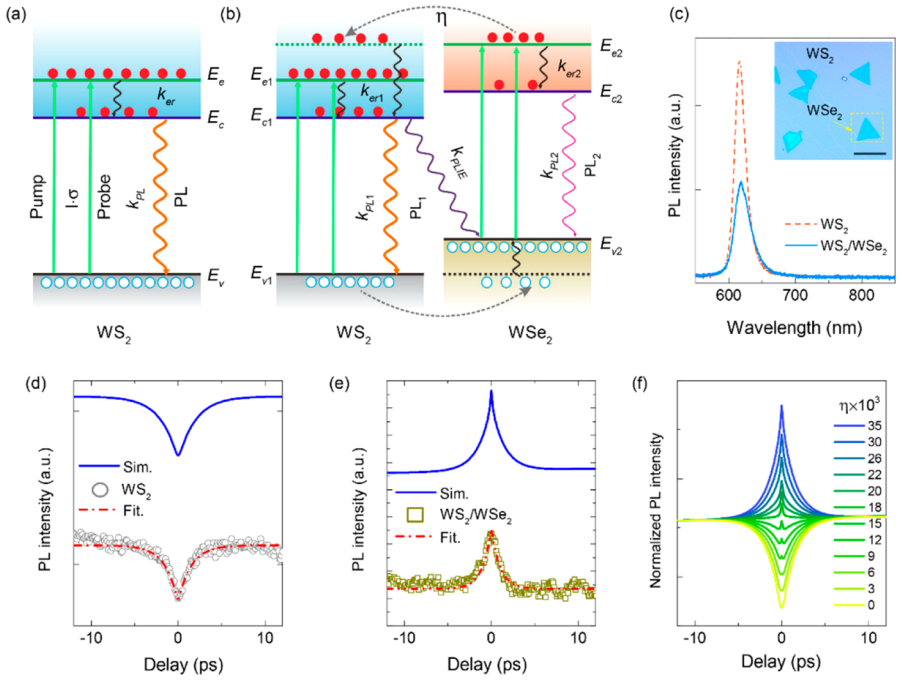

Figure 1. Schematic illustration of a pump−probe photoluminescence (PL) scheme for (a) monolayer WS_2 and (b) WS_2/WSe_2 heterostructures. E_v, E_c, and E_e represent the top of the valence band, the minimum of the conduction band, and the higher excited state of the intraconduction state of monolayer WS_2. E_{v1} (E_{v2}), E_{c1} (E_{c2}), and E_{e1} (E_{e2}) denote the corresponding states of monolayer WS_2 (WSe_2) in the heterostructures. k_{er} (k_{er1} and k_{er2}) represents the cooling rate in monolayer WS_2 (WS_2/WSe_2 heterostructure). k_{PL} (k_{PL1} and k_{PL2}) represents the rate of spontaneous emission of monolayer WS_2 (WS_2 and WSe_2 in the heterostructure), k_{PLIE} represents the emission rate of interlayer excitons. Filled (red) and empty (blue) circles indicate the electrons and holes. (c) PL spectra of monolayer WS_2 and WS_2/WSe_2 heterostructure. The inset shows a photograph of the sample, where a monolayer WS_2 film was fabricated on a Si/SiO_2 substrate; triangle monolayer WSe_2 was then transferred on the top of WS_2. Scale bar: 20 μm. (d and e) Ultrafast pump−probe PL intensity (PL trajectory) as a function of time delay for monolayer WS_2 (circles) and WS_2/WSe_2 (squares), the fits (dash−dot lines) based on eq 5, and the simulations (solid lines) based on the corresponding rate equations, respectively. (f) PL trajectory of the WS_2/WSe_2 heterostructure as a function of η.

demanded after device fabrications. Many efforts have been made during the past few years, including thermal annealing,[22] laser/ion irradiation,[23,24] atomic force microscope (AFM) tip squeezing,[25] and chemical treatment.[26] The second one is establishing criteria to characterize and monitor the interlayer coupling during the tuning processes. So far, the characterizations of the interlayer coupling are often presented as optical,[27] photoluminescence (PL),[28] Raman spectra,[29] and/or AFM imaging.[30] For example, Evgeny *et al.* developed PL imaging in a bright-field optical microscope to identify the layer thickness and track changes in the interlayer coupling during thermal annealing.[31] The Sow group transformed the WS_2/WSe_2 heterostructure from the noncoupling to the strong coupling regime by focused laser treatment and monitored the transforms *via* PL imaging.[32] Matthew *et al.* created clean 2D material interfaces using the AFM tip as a nano "squeegee",[25] demonstrating the result by AFM topography and PL spectra.

These works have made many groundbreaking efforts to enhance and characterize the interlayer coupling. However, these techniques generally present qualitative descriptions and suffer inherent limitations. For example, although AFM imaging exhibits a completely flat topography, the interlayer coupling is still inhomogeneous for the heterostructures (as evident from PL imaging).[25] On the other hand, PL intensity is sensitive to the excitation power and sample quality and, thus, may vary from sample to sample. Considering that the interlayer coupling of vdW heterostructures is associated with the ultrafast electron/energy transfer between different layers, we develop two criteria to assess the interlayer coupling of TMDC heterostructures by using ultrafast pump−probe PL spectroscopy. Based on our physical model, when the coupling tuning from the noninteraction to the strong regime, PL at zero time delay between the pump and probe laser pulses will vary from quench to enhancement. This prediction has been proved in WS_2/WSe_2 heterostructures, where the coupling was modified by thermal annealing. Particularly, the relative PL difference (labeled as ζ) at zero delay time is insensitive to the excitation power and absolute PL intensity, providing a good criterion to assess the coupling among different samples. We also provide another parameter, η, denoting the efficiency of electron transfer between the two monolayers, to quantitatively characterize the interlayer coupling. Our scheme presents a powerful tool for the characterization of the interlayer coupling in TMDC heterostructures, enabling the rational design and development of vdW heterostructure-based electronic and optoelectronic applications with enhanced features and performance.

RESULTS AND DISCUSSION

Theoretical Model. Considering that the interlayer coupling in heterostructures is intrinsically linked to the ultrafast electron transfer between different monolayer materials, the ultrafast dynamics can consistently characterize the interlayer coupling. Here we develop an ultrafast pump−probe PL spectroscopy method to reveal the interlayer coupling of 2D heterostructures, benefiting from the zero-

https://doi.org/10.1021/acsnano.1c01787
ACS Nano 2021, 15, 12966−12974

background feature of the PL technique and the sensitivity of the PL intensity to the interlayer coupling. The schematic diagram of the pump−probe PL spectroscopy to monolayer materials is depicted in Figure 1a, which can be considered as the noncoupling case for 2D heterostructures. The energy diagram is simplified as a three-level system, the top of the valence band (E_v), the minimum of the conduction band (E_c), and the higher excited state of the intraconduction state (E_e). The transitions between E_v and E_e states are coupled *via* the pump and probe laser pulses. PL emission is associated with the transition from E_c to E_v. The electrons will first be excited from E_v to E_e by the pump laser. Then the hot electrons will either be stimulated emission by the probe laser or relax to E_c *via* subsequent thermalization and relaxation with the rate of k_{er}. Here we ignore the influence of the excitation wavelengths (see Supplementary S9). The stimulated emission, with the same wavelength as the pump and probe laser, will be filtered by the dichroic mirror and thus cannot be detected. On the other hand, the cooled electrons will decay spontaneously back to E_v with a rate of k_{PL}, contributing to PL intensity. Note that, in this model, the influence of other quasi-particles (such as charged exciton, defect-bound exciton, and biexciton) has been taken into account in the value of k_{PL}; see Supplementary S7 for details. In this case, the ultrafast processes of monolayer materials can be described with the following coupled rate equations:[33−35]

$$\frac{dN_v(t)}{dt} = -I_L(t)\sigma N_v(t) + I_L(t)\sigma N_e(t) + k_{PL}N_c(t) \quad (1)$$

$$\frac{dN_c(t)}{dt} = k_{er}N_e(t) - k_{PL}N_c(t) \quad (2)$$

$$\frac{dN_e(t)}{dt} = I_L(t)\sigma N_v(t) - I_L(t)\sigma N_e(t) - k_{er}N_e(t) \quad (3)$$

The interpretations for each term have been illustrated in Supplementary S1. Particularly, σ is the absorption cross section of monolayer materials (assumed to be equal for pump and probe processes). $N_v(t)$, $N_c(t)$, and $N_e(t)$ are the time-dependent population in the three states. $I_L(t)$ is the laser intensity at time t. In our experiment, both pump and probe pulses are modeled as Gaussian intensity profiles, $\vec{I}L(t) = \vec{I}\cdot(e^{-t^2/\tau_0^2} + e^{-(t+\Delta t)^2/\tau_0^2})\cdot\sin(\omega_0 t)$, with a certain wavelength ($c/2\pi\omega_0$), a pulse width (τ_0), and a time delay (Δt) between the pump and probe pulses. Generally, the power intensities of pump and probe pulses are set to be equal.

Considering PL photons are emitted from E_c to E_v, the measured PL intensity is proportional to the total population that passes through the E_c state. To this end, we numerically calculated the rate equations integrated over a time interval from before the first pulse until after the second pulse. Taking monolayer WS_2 as an example, the simulation result is presented in Figure 1d (the solid line; the corresponding parameters are listed in Table 1). Note that PL intensity at a relatively long time delay (beyond the time scale of k_{er}), I_{long}, is stable, consistent with previous transient absorption and reflectance spectroscopy.[36,37] While PL intensity at zero time delay, I_0, presents a clear reduction (or quenching). To quantitatively describe the reduction, here we define the relative PL difference ζ as

Table 1. Parameter Values Used in the Simulations to Fit the Pump−Probe PL Spectroscopy of Monolayer WS_2

parameter	value	ref
σ	10^{-18} cm^2	38
k_{er}	1.5 ps	39, 40
k_{PL}	1.0 ns	41, 42
τ_0	400 fs	
P^a	100 μW	
$I\cdot\sigma^b$	3×10^{-3} s^{-1}	

[a]Typical powers used in the experiments are 10 μW to 1 mW. [b]$I\cdot\sigma$ is calculated after considering the wavelength of the femtosecond laser (532 nm), its repetition frequency (80 MHz), and the absorption coefficient of monolayer WS_2 (0.03).[43,44] See Supplementary S3 for details.

$$\zeta = \frac{\Delta I}{I_{long}} = \frac{I_0 - I_{long}}{I_{long}} \quad (4)$$

Hence, ζ is a negative value for monolayer WS_2. This can be well understood as the hot electrons are stimulated to E_v by the probe laser at zero time delay, thus depleting the hot electrons and quenching PL intensity. When the pulse width is significantly smaller than the relaxation time ($1/k_{er}$), the evolution of PL intensity, I_{PL}, as a function of the delay time (Δt) can be described as

$$I_{PL} = (I_0 - I_{long}) \times e^{-k_{er}\cdot|\Delta t|} + I_0 \quad (5)$$

In other words, we can determine the relaxation rate k_{er} by eq 5.

On the basis of this model, we further consider the heterostructures with a strong coupling, regarding the effective electron transfer between different monolayers, as illustrated in Figure 1b. For simplicity of the model, we only account for type II heterostructures (taking WS_2/WSe_2 as the sample in this context) and further assume that (i) the interlayer electron transfer is treated as an instantaneous process because it generally occurs on a time scale shorter than 100 fs,[36] convoluted with the laser pulse width used in our experiment (400 fs); (ii) the absorption coefficient is equal to the simulated emission coefficient, as discussed above; and (iii) PL spectra of the two monolayer materials can be well separated, and we only detect photons from one of them or the interlayer exciton emission (PL of monolayer WS_2 is detected here). In this condition, the rate equations of the monolayer material with a lower E_v state (WS_2 here) can be expressed as

$$\frac{dN_{v1}(t)}{dt} = -I(t)\sigma N_{v1}(t) + I(t)\sigma N_{e1}(t) + k_{PL1}N_{c1}(t) \quad (6)$$

$$\frac{dN_{c1}(t)}{dt} = k_{er1}N_{e1}(t) - k_{PL1}N_c(t) + \eta\cdot I\sigma\cdot N_{v1}(0)\cdot e^{-k_{er1}\cdot|\Delta t|} \quad (7)$$

$$\frac{dN_{e1}(t)}{dt} = I(t)\sigma N_{v1}(t) - I(t)\sigma N_{e1}(t) - k_{er1}N_{e1}(t) \quad (8)$$

Here we ignore the transition of interlayer excitons, due to their slow spontaneous emission rate. η represents the ratio of the transferred electrons over the excited amount ($I\sigma\cdot N_{v1}(0)$). After assuming the thermalization of the transferred electrons following exponential decay behavior, the electron transfer can be expressed as $\eta\cdot I\sigma\cdot N_{v1}(0)\cdot e^{-k_{er1}\cdot|\Delta t|}$; see Supplementary S2 for details. That is, the stronger the coupling, the more the

https://doi.org/10.1021/acsnano.1c01787
ACS Nano 2021, 15, 12966−12974

transferring and the larger the ratio. Assuming η = 0.03 (considering that the quantum yield of monolayer TMDC is between 0.01% and 100%,[45,46] this assumption is reasonable), we determine the PL trajectory (*i.e.*, PL intensity evolution of heterostructures as a function of time delays), as the solid line shown in Figure 1e. Intriguingly, a PL enhancement occurs at zero time delay, and then PL decays to a plateau level. That is, ζ is a positive value for the heterostructure with strong interlayer coupling. This phenomenon is totally different from monolayer WS_2, which can be regarded as a noncoupling case. A phenomenological explanation for the enhancement is that the transferred electrons from monolayer WSe_2 fill up the stimulated electrons by the probe pulse (tip at zero time delay for monolayer WS_2) or even increase the total electrons and thus enhance the PL intensity. Thus, we can instinctively speculate that, with the increasing of the interlayer coupling, PL intensity at zero time delay should be varied from reduction to enhancement. To confirm this assumption, we numerically simulate PL trajectories with different η values, as presented in Figure 1f. The results fully support our hypothesis, except for a sharp peak at zero time delay, arising from the interferometric effect of the laser pulse (Supplementary S8). Thus, we can conclude that both η and ζ can be used as criteria for assessing the interlayer coupling of 2D heterostructures. The parameter of η can quantitatively reveal the interlayer coupling, after calibrating the fundamental parameters (including absorption and emission coefficients and relaxation rates) from the corresponding monolayer materials with the same technique. On the other hand, the parameter of ζ can qualitatively uncover the interlayer coupling, which is more convenient without any further parameters.

Sample Preparation and Optical System. To prove the effectiveness of our model, we performed ultrafast pump–probe PL spectroscopy on the WS_2/WSe_2 heterostructure as well as the monolayer WS_2. The continuous monolayer WS_2 film was fabricated by the chemical vapor deposition (CVD) method on a Si/SiO_2 substrate. Monolayer WSe_2 with a triangular shape, synthesized through CVD on a sapphire substrate, was then transferred to the monolayer WS_2 with a PMMA-assisted method,[47] as shown in Figure 1c. In this case, the presence of residual PMMA molecules and other contaminants is inevitable and thus reduces the interlayer coupling. To tune the coupling and reveal the advantage of our technique, we annealed the heterostructure sample under a vacuum condition with different temperatures and times, as discussed below.

The schematic of the pump–probe optical system is presented in Supplementary S4. Briefly, a vertically polarized sub-picosecond laser (Femto-Fiber pro TVIS, Toptica), with a pulse width of 400 fs at a wavelength of 532 nm, was used as the excitation laser. The pump and probe pulses with a tunable time delay were generated by a homemade Michelson interferometer structure. A linear stage was mounted on one reflection mirror to vary the optical path and thus the time delay between the two pulses. On the other arm, the beam passed through a quarter-wave plate to convert the laser into horizontal polarization. Thus, two beams recombining at the beam splitter have orthogonal polarizations, which can eliminate the two excitation light pulses interfering with each other. In this case, the sharp peak at zero time delay can be removed. Further description can be found in Methods and Supplementary S4.

Ultrafast Pump–Probe PL Spectroscopy of WS_2/WSe_2 Heterostructures. We first performed the ultrafast pump–probe PL spectroscopy on monolayer WS_2, and the result is shown in Figure 1d (the circles). Note that the PL trajectory is in good agreement with the simulation by our model. And also the trajectory can be well fitted by eq 5 (as the dash–dot line shown in Figure 1d). The determined relaxation time is 1.45 ps, consistent with the previous reports.[39,40] We further performed PL spectroscopy on the WS_2/WSe_2 heterostructure, which has been annealed at 525 K for 3 h. The two monolayers have efficient interlayer coupling, evidenced by the quenching of WS_2 PL spectroscopy (Figure 1c), as well as PL quenching of WS_2/WSe_2 heterostructures in their PL imaging (Supplementary S5). The PL trajectory of the heterostructure is presented in Figure 1e (the squares), which agrees reasonably well with the corresponding simulation (the solid line). We can analyze PL decay of the heterostructure by eq 5 as well (the dash–dot line) and demonstrate the relaxation time to be 0.97 ps.

To reveal the robustness of our technique, we further conducted excitation-power-dependent PL spectroscopy of the heterostructures, as shown in Figure 2a. Note that PL

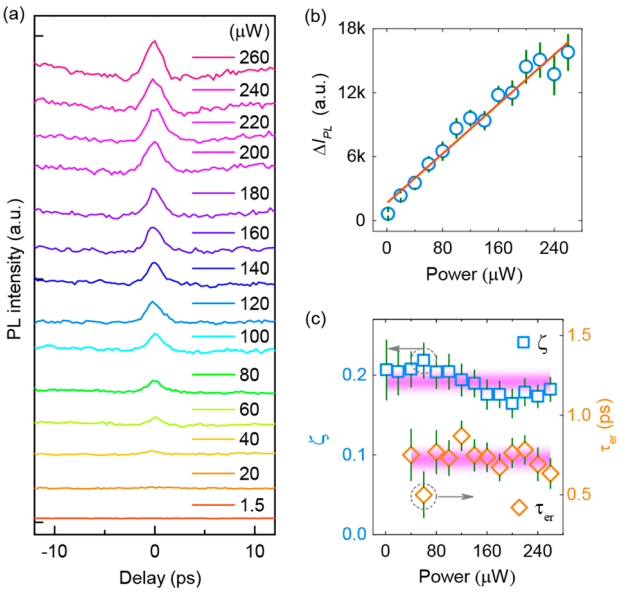

Figure 2. Power-dependent pump–probe PL trajectories and the robustness of ζ. (a) Ultrafast pump–probe PL trajectories as a function of excitation powers. (b) PL difference at the time delay between 0 and 10 ps, ΔI_{PL}, as a function of excitation powers. The solid line is the linear fit, with the correlation coefficients R^2 > 0.98. (c) Relative PL difference, ζ, and the relaxation time, τ_{er}, as a function of excitation powers. The color shadows represent the corresponding averaged values, associated with the standard derivations.

trajectories under different excitation powers have similar profiles, although their absolute intensities rapidly increase with the laser power. The PL difference between the zero time delay (Δt = 0 ps) and the long time delay (Δt = 10 ps used here), $\Delta I_{PL} = I_0 - I_{long}$, as a function of exciton powers is depicted in Figure 2b. We can find that the PL difference scales linearly with the excitation powers (the solid line is the linear fitting), indicating the PL difference is insensitive to excitation powers. This conclusion can be further supported by the ignorable change of the relative PL difference, ζ, as the squares

https://doi.org/10.1021/acsnano.1c01787
ACS Nano 2021, 15, 12966–12974

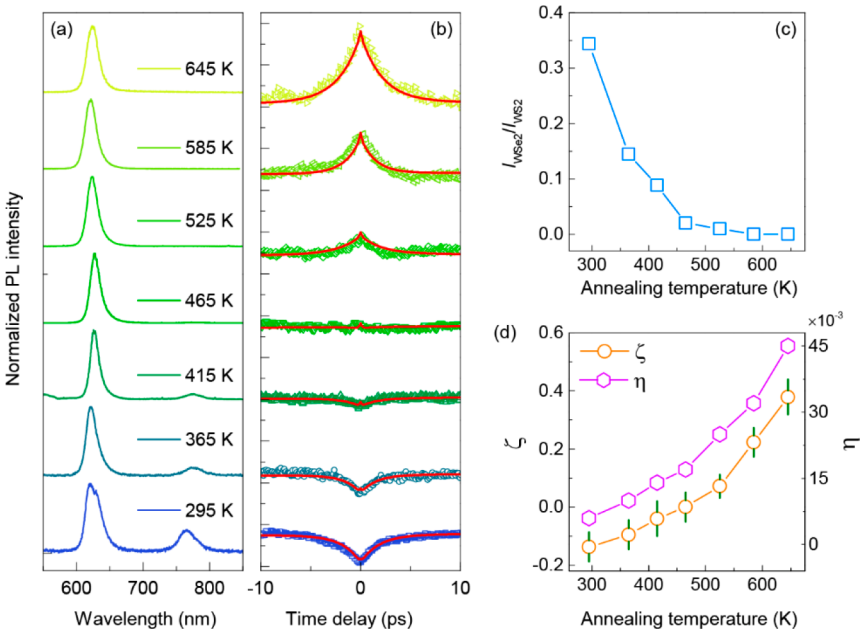

Figure 3. Assessing the interlayer coupling of the heterostructure *via* η and ζ. Spectra and parameters as a function of annealing temperatures. (a) PL spectra of the WS_2/WSe_2 heterostructure, (b) ultrafast pump−probe PL trajectories, (c) integrated PL intensity ratio of WSe_2 (I_{WSe2}) to WS_2 (I_{WS2}), (d) the determined relative PL difference, ζ, and the simulated electron transfer ratio, η. The solid lines are the simulation results. The corresponding parameters are listed in Table S1.

shown in Figure 2c. We also determine the relaxation time by eq 5 (the diamonds shown in Figure 2c). The slight variation might result from the fluctuation of PL intensity and the low signal-to-noise ratio, which can be solved by increasing the integration time. One may also note that, under high power excitation (such as 240 and 260 μW), PL trajectories present slight downward profiles around short time delays, and ζ emerges a mild variation. We tentatively attribute these phenomena to the nonlinear optical behaviors (such as saturation absorption) or many-body interactions (such as exciton−exciton annihilation) in the WS_2/WSe_2 heterostructure.

Assessing the Interlayer Coupling of the Heterostructures *via* ζ and η. To illustrate the availability of ζ and η as the criteria for assessing the interlayer coupling of 2D heterostructures, we performed ultrafast pump−probe PL measurements with tunable interlayer coupling. As discussed above, the interlayer coupling can be tuned by thermal annealing,[22] laser/ion irradiation,[23,24] and tip squeezing.[25] Here we modified the coupling of the WS_2/WSe_2 heterostructure by thermal annealing under a high vacuum. PL spectroscopy varied as the annealing temperatures is presented in Figure 3a (the annealing times were all 3 h). As compared to PL of monolayer WS_2, the reduction of WSe_2 indicates the increase of the interlayer coupling with the increase of the annealing temperature. Consequently, the PL intensity ratio of WSe_2 to WS_2 has been regarded as a criterion of the interlayer coupling previously.[48] However, with the annealing temperature further increased (such as T > 465 K), PL spectra of WSe_2 are fully quenched, as shown in Figure 3a and c. In this case, the PL intensity ratio is invalid to characterize the coupling. Note that although the spectra of WSe_2 fully disappeared with an annealing temperature larger than 465 K, both WSe_2 and WS_2/WSe_2 heterostructures can be well maintained until 725 K, evidenced by their Raman spectra (Supplementary S6). On the other hand, ultrafast pump−probe PL trajectories under different annealing temperatures present obvious changes, where PL intensity at the zero time delay varied from the quenched to the enhanced results (Figure 3b). That is to say, with the increase of interlayer coupling, the PL difference (ΔI_{PL}) and the corresponding parameter of ζ vary from negative to positive values (Figure 3d), consistent with our assumption. Therefore, we can declare that the parameter of ζ can be regarded as a criterion to assess the interlayer coupling. To further quantitatively assess the interlayer coupling, we simulate the pump−probe PL trajectory evolution as a function of the parameter η by eqs 6 to 8, as the solid lines shown in Figure 3b. The determined η presented in Figure 3d shows similar behavior to the parameter of ζ, indicating the effectiveness and consistency of our criteria.

Our technique also provides a scheme to image the interlayer coupling of heterostructures. Considering that performing the pump−probe PL trajectory for each pixel is time-consuming, we offer an alternative scheme by carrying out the pump−probe PL imaging (Im) at two delay times, Δt = 0 ps ($Im_{t=0}$) and Δt = 10 ps ($Im_{t=10}$), respectively. Then a difference imaging (ΔIm) can be determined by subtracting the above two imagings, $\Delta Im = Im_{t=0} - Im_{t=10}$. Consequently, the interlayer coupling imaging (Im_ζ) can be obtained *via* dividing the difference imaging by the PL imaging at a time delay of 10 ps, *i.e.*, $Im_\zeta = \Delta Im/Im_{t=10}$. In this case, the interlayer coupling can be readily determined, as shown in Figure 4. Although the residual organics and other contaminants may exist in the as-prepared sample, a weak interlayer coupling is still present in the WS_2/WSe_2 heterostructure (Figure 4a). This can be evidenced by PL intensities of WS_2/WSe_2 (2085 cps, see Figure S5 for the statistical results) weaker than that of bare WS_2 (2472 cps) at the time delay of 10 ps. When we excited the sample by the two pulses at zero time delay, as expected, PL intensities of both heterostructure (1785 cps) and monolayer WS_2 (2083 cps) are quenched, as presented in Figure 4b. Consequently,

https://doi.org/10.1021/acsnano.1c01787
ACS Nano 2021, 15, 12966−12974

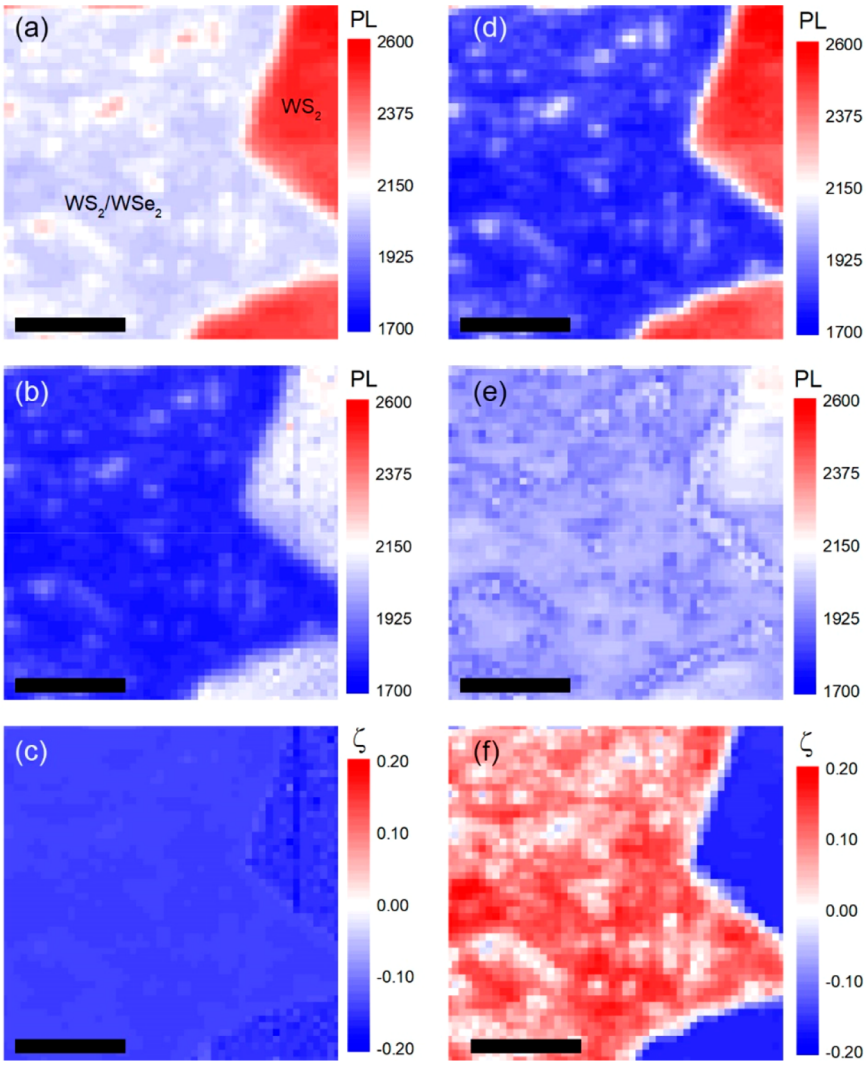

Figure 4. Imaging the interlayer coupling of the WS_2/WSe_2 heterostructure *via* the relative PL difference, ζ. (a and b) PL imaging of the as-prepared heterostructure at the time delay of 10 and 0 ps, respectively. The areas of monolayer WS_2 and WS_2/WSe_2 heterostructures have been marked in the figures. (c) Corresponding interlayer coupling imaging *via* ζ for the as-prepared sample. (d and e) PL imaging of the heterostructures after thermal annealing at 525 K for 3 h at the time delay of 10 and 0 ps, respectively. (f) Corresponding interlayer coupling imaging for the annealed sample. Scale bars: 10 μm.

the average values of ζ for WS_2/WSe_2 (−0.143) are only slightly larger than that of monolayer WS_2 (−0.154), indicating the weaker interlayer coupling of heterostructures. After annealing at 525 K for 3 h, the variation of PL intensity of monolayer WS_2 at a time delay of 10 ps (2458 cps) can be ignored, while that of WS_2/WSe_2 presents a significant reduction (1812 cps), due to the enhanced electron transfer between the two monolayers. On the other hand, at zero time delay, monolayer WS_2 and the WS_2/WSe_2 heterostructure present similar PL intensity (1994 *vs* 2094) and thus cannot be well distinguished from PL imaging. In this case, ζ for monolayer WS_2 presents an insignificant change (−0.163), while ζ for the WS_2/WSe_2 heterostructure varies from the negative to a positive value (0.09), hinting that the interlayer coupling has been dramatically enhanced after thermal annealing. To further prove the effectiveness of our technique to track the interlayer coupling of vdW heterostructures, we displayed the Im_ζ imaging of another WS_2/WSe_2 heterostructure after annealing with a series of temperatures (from 295 to 575 K; see Supplementary S11), and the results are in reasonable agreement with the predictions. Furthermore, we also performed the ultrafast PL measurements on the MoS_2/WS_2 heterostructures (Supplementary, S12),; the result is also in accord with the WS_2/WSe_2 heterostructures, proving the universality of our technique.

Here we provide two parameters, which can act as criteria to evaluate the interlayer coupling of the TMDC heterostructures. To improve our technique, further experimental and theoretical investigations are needed. First, some hypotheses have been adopted to simplify the simulation, such as assuming the same absorption and stimulated emission coefficients of monolayer materials and their heterostructures, ignoring the time of charge transfer between the heterostructures and the pulse width of the excitation laser. These parameters may significantly influence the resulting pump−probe PL trajectory and thus the two criteria. Taking η as an example, according to its definition (the ratio of transferred electrons over the total excited electrons), the value of η is between 0 and 1. However, it may be larger than the one in our simulation, because we assume the number of excited electrons of monolayer WS_2 and

https://doi.org/10.1021/acsnano.1c01787
ACS Nano 2021, 15, 12966−12974

WSe_2 is the same, while that of WSe_2 may be much larger than WS_2. Thus, these parameters (including spontaneous emission coefficients of intralayer and interlayer excitons and the nonradiative rates) should be accurately supplied to determine the optimized criterion. Second, the quantitative parameter of η is determined by the simulation of PL trajectories. However, measuring the pump−probe PL trajectories of the heterostructures is time-consuming, and η cannot be accurately determined through simulations. These two limitations should be overcome for practical applications. Third, for 2D heterostructures where PL spectra of the two different materials cannot be well separated, all the relevant energy levels should be taken into account. The much more sophisticated rate equation set complicates the task of theoretical simulations and experimental data analysis. In this case, advanced theoretical works may be performed to simplify the physical model and to extract criteria. Last, this model so far is incapable of the heterostructure without significant PL emission (taking graphene/BN as an example). Therefore, it is also necessary to modify the physical model and develop a similar transient absorption scheme to evaluate the interlayer coupling.

CONCLUSIONS

Here we provide two criteria to assess the interlayer coupling of TMDC heterostructures by considering the electron transfer between the two monolayers in heterostructures and numerically calculating the rate equations. The ratio of transferred electrons over the total excited electrons, η, offers a quantitative criterion to evaluate the interlayer coupling. The relative PL difference at different time delays between the pump and probe pulses, ζ, affords a qualitative criterion of the interlayer coupling. We have proved the effectiveness of two criteria by varying the interlayer coupling of WS_2/WSe_2 heterostructures through thermal annealing and measuring the pump−probe PL trajectory of monolayer WS_2. The value of η, determined by comparison of the measured results and the numerical simulations, varies from 0.001 to 0.045. Furthermore, the value of ζ, determined by comparison of PL intensity at time delays between 0 and 10 ps, changes from a negative value (−0.137) to a positive value (0.379). We have further provided that these two criteria are robust and insensitive to the excitation power in a broad power region. We also create a scheme to image the interlayer coupling by performing PL imaging at two selected time delays. Our criteria developed in this work enable a powerful technique to characterize the interlayer coupling of TMDC heterostructures and allows the reproducible fabrications of vdW heterostructures, which can boost the practical applications of electronic and optoelectronic devices based on 2D heterostructured materials.

METHODS

The experiment setup is sketched in Figure S4. The polarized subpicosecond laser was split by a beam splitter with an intensity ratio of 50:50 (BS_1) to obtain two laser pulses with the same power. On one optical arm, the laser passed through a quarter-wave plate ($\lambda/4$) used for polarization rotation. On the other arm, the optical path can be continuously changed by the linear stage installed under the mirror (M). Thus, the time delay (Δt) between the two pulses can be tuned finely. The combined laser beam was further split by another BS with a ratio of 10:90 (BS_2). After a polarizer, the weaker beam was monitored by a high-speed photodetector (PD, HCA-S-400M-SI) to calibrate the time delays. The stronger beam was reflected into the objective (OBJ, Olympus LMPlanFLN, 100×) lens *via* a dichroic mirror (DM, Semrock, Di02-R532-25x36), and then the laser was focused onto the prepared sample. The diameter of the laser spot is close to the diffraction limit (~400 nm). The vdW heterostructures were placed on an XY piezo scanner (PiezoSystem Jena,PXY 102 SG). PL imagings were achieved by moving the sample with respect to the laser spot in a controlled way. The step size was generally set to 300 nm. The time-dependent PL from the sample was collected by the same OBJ, transmitted through the DM and a short-pass filter (SP), and finally detected by a single-photon counting modulator (SPCM, PcoQuant τ−SPAD-50). Then the data were transferred to the computer for further data processing.

ASSOCIATED CONTENT

Supporting Information

The Supporting Information is available free of charge at https://pubs.acs.org/doi/10.1021/acsnano.1c01787.

Interpretations of the rate equations for eqs 1−3 and 6−8, respectively (S1 and S2); derivation of parameters of rate equations (S3); optical schematic (S4); optical characterizations of the WS_2/WSe_2 heterostructures (S5 and S6); influences of the quasi-particles, pulse widths, excitation wavelengths on the ultrafast response (S7−S9); determining ζ under different conditions (S10); imaging the interlayer coupling after annealing with different temperatures (S11); ultrafast response of MoS_2/WS_2 heterostructures (S12); and simulation parameters for Figure 3b (Table S1) (PDF)

AUTHOR INFORMATION

Corresponding Authors

Chengbing Qin − *State Key Laboratory of Quantum Optics and Quantum Optics Devices, Institute of Laser Spectroscopy and Collaborative Innovation Center of Extreme Optics, Shanxi University, Taiyuan, Shanxi 030006, China;* orcid.org/0000-0002-6822-5113; Email: chbqin@sxu.edu.cn

Liantuan Xiao − *State Key Laboratory of Quantum Optics and Quantum Optics Devices, Institute of Laser Spectroscopy and Collaborative Innovation Center of Extreme Optics, Shanxi University, Taiyuan, Shanxi 030006, China;* orcid.org/0000-0003-2690-6460; Email: xlt@sxu.edu.cn

Authors

Shuangping Han − *State Key Laboratory of Quantum Optics and Quantum Optics Devices, Institute of Laser Spectroscopy and Collaborative Innovation Center of Extreme Optics, Shanxi University, Taiyuan, Shanxi 030006, China*

Xilong Liang − *State Key Laboratory of Quantum Optics and Quantum Optics Devices, Institute of Laser Spectroscopy and Collaborative Innovation Center of Extreme Optics, Shanxi University, Taiyuan, Shanxi 030006, China*

Yan Gao − *Department of Physics, Shanxi Datong University, Datong, Shanxi 037009, China*

Yunrui Song − *State Key Laboratory of Quantum Optics and Quantum Optics Devices, Institute of Laser Spectroscopy and Collaborative Innovation Center of Extreme Optics, Shanxi University, Taiyuan, Shanxi 030006, China*

Shen Wang − *College of Physics and Electronics Engineering, Shanxi University, Taiyuan, Shanxi 030006, China*

Xingliang Su − *College of Physics and Electronics Engineering, Shanxi University, Taiyuan, Shanxi 030006, China*

Guofeng Zhang − *State Key Laboratory of Quantum Optics and Quantum Optics Devices, Institute of Laser Spectroscopy*

and Collaborative Innovation Center of Extreme Optics, Shanxi University, Taiyuan, Shanxi 030006, China; orcid.org/0000-0002-9030-0431

Ruiyun Chen − *State Key Laboratory of Quantum Optics and Quantum Optics Devices, Institute of Laser Spectroscopy and Collaborative Innovation Center of Extreme Optics, Shanxi University, Taiyuan, Shanxi 030006, China;* orcid.org/0000-0002-0037-856X

Jianyong Hu − *State Key Laboratory of Quantum Optics and Quantum Optics Devices, Institute of Laser Spectroscopy and Collaborative Innovation Center of Extreme Optics, Shanxi University, Taiyuan, Shanxi 030006, China*

Mingyong Jing − *State Key Laboratory of Quantum Optics and Quantum Optics Devices, Institute of Laser Spectroscopy and Collaborative Innovation Center of Extreme Optics, Shanxi University, Taiyuan, Shanxi 030006, China*

Suotang Jia − *State Key Laboratory of Quantum Optics and Quantum Optics Devices, Institute of Laser Spectroscopy and Collaborative Innovation Center of Extreme Optics, Shanxi University, Taiyuan, Shanxi 030006, China*

Complete contact information is available at: https://pubs.acs.org/10.1021/acsnano.1c01787

Author Contributions

C.Q. and L.X. designed and supervised the experiments. S.H., X.L., Y.G., and Y.S. carried out the optical experiments. S.H. and Y.S. annealed the heterostructures. S.W. and X.S. characterized the prepared samples. J.H. and M.J. were responsible for laser management. G.Z., R.C., and S.J. contributed to the data analysis. S.H., C.Q., and X.L. wrote the manuscript. All authors commented on the manuscript.

Notes

The authors declare no competing financial interest.

ACKNOWLEDGMENTS

The authors gratefully acknowledge support from the National Key Research and Development Program of China (Grant No. 2017YFA0304203), Natural Science Foundation of China (Nos. 91950109, 61875109, 62075120, 62075122, 62005150, and 62011530047), Natural Science Foundation of Shanxi Province (No. 201901D111010(ZD)), PCSIRT (No. IRT_17R70), 111 projects (Grant No. D18001), 1331KSC, PTIT, and Postgraduate Education Innovation Project of Shanxi Province (No. 2019SY047).

REFERENCES

(1) Wang, G.; Chernikov, A.; Glazov, M. M.; Heinz, T. F.; Marie, X.; Amand, T.; Urbaszek, B. Colloquium: Excitons in Atomically Thin Transition Metal Dichalcogenides. *Rev. Mod. Phys.* **2018**, *90*, 021001.

(2) Xu, X.; Yao, W.; Xiao, D.; Heinz, T. F. Spin and Pseudospins in Layered Transition Metal Dichalcogenides. *Nat. Phys.* **2014**, *10*, 343−350.

(3) Chhowalla, M.; Shin, H. S.; Eda, G.; Li, L. J.; Loh, K. P.; Zhang, H. The Chemistry of Two-Dimensional Layered Transition Metal Dichalcogenide Nanosheets. *Nat. Chem.* **2013**, *5*, 263−275.

(4) Qin, C.; Gao, Y.; Qiao, Z.; Xiao, L.; Jia, S. Atomic Layered MoS_2 As a Tunable Optical Platform. *Adv. Opt. Mater.* **2016**, *4*, 1429.

(5) Zereshki, P.; Wei, Y.; Long, R.; Zhao, H. Layer-Coupled States Facilitate Ultrafast Charge Transfer in a Transition Metal Dichalcogenide Trilayer Heterostructure. *J. Phys. Chem. Lett.* **2018**, *9*, 5970−5978.

(6) Novoselov, K. S.; Mishchenko, A.; Carvalho, A.; Castro Neto, A. H. 2D Materials and van der Waals Heterostructures. *Science* **2016**, *353*, aac9439.

(7) Geim, A. K.; Grigorieva, I. V. Van der Waals Heterostructures. *Nature* **2013**, *499*, 419−425.

(8) Ponomarenko, L. A.; Gorbachev, R. V.; Yu, G. L.; Elias, D. C.; Jalil, R.; Patel, A. A.; Mishchenko, A.; Mayorov, A. S.; Woods, C. R.; Wallbank, J. R.; Mucha-Kruczynski, M.; Piot, B. A.; Potemski, M.; Grigorieva, I. V.; Novoselov, K. S.; Guinea, F.; Fal'ko, V. I.; Geim, A. K. Cloning of Dirac Fermions in Graphene Superlattices. *Nature* **2013**, *497*, 594−597.

(9) Britnell, L.; Gorbachev, R. V.; Jalil, R.; Belle, B. D.; Schedin, F.; Mishchenko, A.; Georgiou, T.; Katsnelson, M. I.; Eaves, L.; Morozov, S. V.; Peres, N. M. R.; Leist, J.; Geim, A. K.; Novoselov, K. S.; Ponomarenko, L. A. Field-Effect Tunneling Transistor Based on Vertical Graphene Heterostructures. *Science* **2012**, *335*, 947−950.

(10) Fiori, G.; Bonaccorso, F.; Iannaccone, G.; Palacios, T.; Neumaier, D.; Seabaugh, A.; Banerjee, S. K.; Colombo, L. Electronics Based on Two-Dimensional Materials. *Nat. Nanotechnol.* **2014**, *9*, 768−779.

(11) Yu, W. J.; Liu, Y.; Zhou, H.; Yin, A.; Li, Z.; Huang, Y.; Duan, X. Highly Efficient Gate-Tunable Photocurrent Generation in Vertical Heterostructures of Layered Materials. *Nat. Nanotechnol.* **2013**, *8*, 952−958.

(12) Alexeev, E. M.; Catanzaro, A.; Skrypka, O. V.; Nayak, P. K.; Ahn, S.; Pak, S.; Lee, J.; Sohn, J. I.; Novoselov, K. S.; Shin, H. S.; Tartakovskii, A. I. Imaging of Interlayer Coupling in van der Waals Heterostructure Using a Bright-Field Optical Microscope. *Nano Lett.* **2017**, *17*, 5342−5349.

(13) Uwanno, T.; Hattori, Y.; Taniguchi, T.; Watanabe, K.; Nagashio, K. Fully Dry PMMA Transfer of Graphene on h-BN Using a Heating/cooling System. *2D Mater.* **2015**, *2*, 041002.

(14) Park, H.; Shin, G. H.; Lee, K. J.; Choi, S.-Y. Probing Temperature-Dependent Interlayer Coupling in a MoS_2/h-BN Heterostructure. *Nano Res.* **2020**, *13*, 576−582.

(15) Xu, W.; Liu, W.; Schmidt, J. F.; Zhao, W.; Lu, X.; Raab, T.; Diederichs, C.; Gao, W.; Seletskiy, D. V.; Xiong, Q. Correlated Fluorescence Blinking in Two-Dimensional Semiconductor Heterostructures. *Nature* **2017**, *541*, 62−67.

(16) Sanchez, D. A.; Dai, Z.; Wang, P.; Cantu-Chavez, A.; Brennan, C. J.; Huang, R.; Lu, N. Mechanics of Spontaneously Formed Nanoblisters Trapped by Transferred 2D Crystals. *Proc. Natl. Acad. Sci. U. S. A.* **2018**, *115*, 7884−7889.

(17) Khestanova, E.; Guinea, F.; Fumagalli, L.; Geim, A. K.; Grigorieva, I. V. Universal Shape and Pressure inside Bubbles Appearing in van der Waals Heterostructures. *Nat. Commun.* **2016**, *7*, 12587.

(18) Liu, N.; Pan, Z.; Fu, L.; Zhang, C.; Dai, B.; Liu, Z. The Origin of Wrinkles on Transferred Graphene. *Nano Res.* **2011**, *4*, 996−1004.

(19) Pak, S.; Lee, J.; Lee, Y. W.; Jang, A. R.; Ahn, S.; Ma, K. Y.; Cho, Y.; Hong, J.; Lee, S.; Jeong, H. Y.; Im, H.; Shin, H. S.; Morris, S. M.; Cha, S.; Sohn, J. I.; Kim, J. M. Strain-Mediated Interlayer Coupling Effects on the Excitonic Behaviors in an Epitaxially Grown MoS_2/WS_2 van der Waals Heterobilayer. *Nano Lett.* **2017**, *17*, 5634−5640.

(20) Nayak, G.; Lisi, S.; Liu, W. L.; Jakubczyk, T.; Stepanov, P.; Donatini, F.; Watanabe, K.; Taniguchi, T.; Bid, A.; Kasprzak, J.; Richard, M.; Bouchiat, V.; Coraux, J.; Marty, L.; Bendiab, N.; Renard, J. Cathodoluminescence Enhancement and Quenching in Type-I van der Waals Heterostructures: Cleanliness of the Interfaces and Defect Creation. *Phys. Rev. Mater.* **2019**, *3*, 114001.

(21) Surrente, A.; Dumcenco, D.; Yang, Z.; Kuc, A.; Jing, Y.; Heine, T.; Kung, Y. C.; Maude, D. K.; Kis, A.; Plochocka, P. Defect Healing and Charge Transfer-Mediated Valley Polarization in MoS_2/$MoSe_2$/MoS_2 Trilayer van der Waals Heterostructures. *Nano Lett.* **2017**, *17*, 4130−4136.

(22) Mouri, S.; Zhang, W.; Kozawa, D.; Miyauchi, Y.; Eda, G.; Matsuda, K. Thermal Dissociation of Inter-Layer Excitons in MoS_2/$MoSe_2$ Hetero-Bilayers. *Nanoscale* **2017**, *9*, 6674−6679.

(23) Miyamoto, Y.; Zhang, H.; Miyazaki, T.; Rubio, A. Modifying the Interlayer Interaction in Layered Materials with an Intense IR Laser. *Phys. Rev. Lett.* **2015**, *114*, 116102.

(24) Tan, Y.; Liu, X.; He, Z.; Liu, Y.; Zhao, M.; Zhang, H.; Chen, F. Tuning of Interlayer Coupling in Large-Area Graphene/WSe_2 van der Waals Heterostructure *via* Ion Irradiation: Optical Evidences and Photonic Applications. *ACS Photonics* **2017**, *4*, 1531−1538.
(25) Rosenberger, M. R.; Chuang, H. J.; McCreary, K. M.; Hanbicki, A. T.; Sivaram, S. V.; Jonker, B. T. Nano-"Squeegee" for the Creation of Clean 2D Material Interfaces. *ACS Appl. Mater. Interfaces* **2018**, *10*, 10379.
(26) Ji, J.; Delehey, C. M.; Houpt, D. N.; Heighway, M. K.; Lee, T.; Choi, J. H. Selective Chemical Modulation of Interlayer Excitons in Atomically Thin Heterostructures. *Nano Lett.* **2020**, *20*, 2500−2506.
(27) Wang, K.; Huang, B.; Tian, M.; Ceballos, F.; Lin, M.-W.; Mahjouri-Samani, M.; Boulesbaa, A.; Puretzky, A. A.; Rouleau, C. M.; Yoon, M.; Zhao, H.; Xiao, K.; Duscher, G.; Geohegan, D. B. Interlayer Coupling in Twisted WSe_2/WS_2 Bilayer Heterostructures Revealed by Optical Spectroscopy. *ACS Nano* **2016**, *10*, 6612−6622.
(28) Tongay, S.; Fan, W.; Kang, J.; Park, J.; Koldemir, U.; Suh, J.; Narang, D. S.; Liu, K.; Ji, J.; Li, J.; Sinclair, R.; Wu, J. Tuning Interlayer Coupling in Large-Area Heterostructures with CVD-Grown MoS_2 and WS_2 Monolayers. *Nano Lett.* **2014**, *14*, 3185−3190.
(29) Ding, L.; Ukhtary, M. S.; Chubarov, M.; Choudhury, T. H.; Zhang, F.; Yang, R.; Zhang, A.; Fan, J. A.; Terrones, M.; Redwing, J. M.; Yang, T.; Li, M.; Saito, R.; Huang, S. Understanding Interlayer Coupling in TMD-hBN Heterostructure by Raman Spectroscopy. *IEEE Trans. Electron Devices* **2018**, *65*, 4059−4067.
(30) Li, L. H.; Tian, T.; Cai, Q.; Shih, C.-J.; Santos, E. J. G. Asymmetric Electric Field Screening in van der Waals Heterostructures. *Nat. Commun.* **2018**, *9*, 1271.
(31) Alexeev, E. M.; Catanzaro, A.; Skrypka, O. V.; Nayak, P. K.; Ahn, S.; Pak, S.; Lee, J.; Sohn, J. I.; Novoselov, K. S.; Shin, H. S.; Tartakovskii, A. I. Imaging of Interlayer Coupling in van der Waals Heterostructures Using a Bright-Field Optical Microscope. *Nano Lett.* **2017**, *17*, 5342−5349.
(32) Lee, Y. Y.; Hu, Z.; Wang, X.; Sow, C.-H. Progressive Micromodulation of Interlayer Coupling in Stacked WS_2/WSe_2 Heterobilayers Tailored by a Focused Laser Beam. *ACS Appl. Mater. Interfaces* **2018**, *10* (43), 37396−37406.
(33) Van Dijk, E. M. H. P.; Hernando, J.; García-López, J.-J.; Crego-Calama, M.; Reinhoudt, D. N.; Kuipers, L.; García-Parajó, M. F.; van Hulst, N. F. Single-Molecule Pump-Probe Detection Resolves Ultrafast Pathways in Individual and Coupled Quantum Systems. *Phys. Rev. Lett.* **2005**, *94*, 078302.
(34) Van Dijk, E.; Hernando, J.; Garcia-Parajo, M. F.; van Hulst, N. F. Single-Molecule Pump-Probe Experiments Reveal Variations in Ultrafast Energy Redistribution. *J. Chem. Phys.* **2005**, *123*, 064703.
(35) Wang, H.; Zhang, C.; Rana, F. Ultrafast Dynamics of Defect-Assisted Electron-Hole Recombination in Monolayer MoS_2. *Nano Lett.* **2015**, *15* (1), 339−345.
(36) Chen, H.; Wen, X.; Zhang, J.; Wu, T.; Gong, Y.; Zhang, X.; Yuan, J.; Yi, C.; Lou, J.; Ajayan, P. M.; Zhuang, W.; Zhang, G.; Zheng, J. Ultrafast Formation of Interlayer Hot Excitons in Atomically Thin MoS_2/WS_2 Heterostructures. *Nat. Commun.* **2016**, *7*, 12512.
(37) He, J.; Kumar, N.; Bellus, M. Z.; Chiu, H. Y.; He, D.; Wang, Y.; Zhao, H. Electron Transfer and Coupling in Graphene-Tungsten Disulfide van der Waals Heterostructures. *Nat. Commun.* **2014**, *5*, 5622.
(38) Zhao, S.; He, D.; He, J.; Zhang, X.; Yi, L.; Wang, Y.; Zhao, H. Probing Excitons in Transition Metal Dichalcogenides by Drude-Like Exciton Intraband Absorption. *Nanoscale* **2018**, *10*, 9538−9546.
(39) Danovich, M.; Aleiner, I. L.; Drummond, N. D.; Fal'ko, V. I. Fast Relaxation of Photo-Excited Carriers in 2-D Transition Metal Dichalcogenides. *IEEE J. Sel. Top. Quantum Electron.* **2017**, *23*, 5.
(40) Vega-Mayoral, V.; Vella, D.; Borzda, T.; Prijatelj, M.; Tempra, I.; Pogna, E. A. A.; Dal Conte, S.; Topolovsek, P.; Vujicic, N.; Cerullo, G.; Mihailovic, D.; Gadermaier, C. Exciton and Charge Carrier Dynamics in Few-Layer WS_2. *Nanoscale* **2016**, *8*, 5428−5434.
(41) Ceballos, F.; Ju, M.-G.; Lane, S. D.; Zeng, X. C.; Zhao, H. Highly Efficient and Anomalous Charge Transfer in van der Waals Trilayer Semiconductors. *Nano Lett.* **2017**, *17*, 1623−1628.
(42) Peimyoo, N.; Shang, J.; Cong, C.; Shen, X.; Wu, X.; Yeow, E. K. L.; Yu, T. Nonblinking, Intense Two-Dimensional Light Emitter: Monolayer WS_2 Triangles. *ACS Nano* **2013**, *7*, 10985−10994.
(43) Zhu, B.; Chen, X.; Cui, X. Exciton Binding Energy of Monolayer WS_2. *Sci. Rep.* **2015**, *5*, 9218.
(44) Mak, K. F.; Lee, C.; Hone, J.; Shan, J.; Heinz, T. F. Atomically Thin MoS_2: A New Direct-Gap Semiconductor. *Phys. Rev. Lett.* **2010**, *105*, 136805.
(45) Qin, C.-B.; Liang, X.-L.; Han, S.-P.; Zhang, G.-F.; Chen, R.-Y.; Hu, J.-Y.; Xiao, L.-T.; Jia, S.-T. Giant Enhancement of Photoluminescence Emission in Monolayer WS_2 by Femtosecond Laser Irradiation. *Front. Phys.* **2021**, *16*, 12501.
(46) Amani, M.; Lien, D. H.; Kiriya, D.; Xiao, J.; Azcatl, A.; Noh, J.; Madhvapathy, S. R.; Addou, R.; Santosh, K. C.; Dubey, M. Near-Unity Photoluminescence Quantum Yield in MoS_2. *Science* **2015**, *350*, 1065−1068.
(47) Liu, Y.; Zhang, S.; He, J.; Wang, Z. M.; Liu, Z. Recent Progress in the Fabrication, Properties, and Devices of Heterostructures Based on 2D Materials. *Nano-Micro Lett.* **2019**, *11*, 13.
(48) Rigosi, A. F.; Hill, H. M.; Li, Y.; Chernikov, A.; Heinz, T. F. Probing Interlayer Interactions in Transition Metal Dichalcogenide Heterostructures by Optical Spectroscopy: MoS_2/WS_2 and $MoSe_2/WSe_2$. *Nano Lett.* **2015**, *15*, 5033−5038.

https://doi.org/10.1021/acsnano.1c01787
ACS Nano 2021, 15, 12966−12974